Cross Sections and Swarm Coefficients for Nitrogen Ions and Neutrals in N_2 and Argon Ions and Neutrals in Ar for Energies from 0.1 eV to 10 keV

A. V. Phelps

Joint Institute for Laboratory Astrophysics, University of Colorado and National Institute of Standards and Technology, Boulder, Colorado 80309-0440

Received May 2, 1990; revised manuscript received October 4, 1990

Graphical and tabulated data and the associated bibliography are presented for cross sections for elastic, excitation, and ionization collisions of N^+, N_2^+, N, and N_2 with N_2 and for Ar^+ and Ar with Ar for laboratory energies from 0.1 eV to 10 keV. Where appropriate, drift velocities and reaction or excitation coefficients are calculated from the cross sections and recommended for use in analyses of swarm experiments and electrical discharges. In the case of N^+ in N_2, cross sections for momentum transfer, charge transfer, electronic excitation, and electron production are recommended. Drift velocity calculations predict runaway for N^+ in N_2 for electric field to gas density ratios E/n greater than 4.3×10^3 Td, where 1 Td (townsend) $= 10^{-21}$ V m^2. For N_2^+ in N_2, the cross sections include those for N^+ and N_3^+ formation, electronic excitation, and electron production. Drift velocities and average cross sections are calculated for $E/n \geqslant 500$ Td. In the case of N in N_2, only cross sections for momentum transfer are recommended. For N_2 in N_2, cross sections for momentum transfer, electronic excitation, and electron production are recommended. Collisions of electronically excited states with N_2 are not included. For Ar^+ in Ar, cross sections for charge transfer, electronic excitation, and electron production are recommended. For Ar in Ar, cross sections for momentum transfer, electronic excitation, and electron production are recommended.

Key words: argon; charge transfer; cross section; data compilation; dissociation; electronic excitation; electron production; emission; fast neutrals; ionization; ions; momentum transfer; nitrogen; rotational excitation; swarm coefficient; vibrational excitation.

Contents

List of Tables

List of Figures

1. Introduction

This paper presents graphical and tabulated data and the associated bibliography for cross sections for elastic, excitation, and ionization collisions of N^+, N_2^+, N, and N_2 in N_2 and for Ar^+, Ar_2^+, and Ar in Ar for laboratory energies from 0.1 eV to 10 keV. Ion transport and reaction coefficients calculated from these cross sections are compared with available experimental data and are tabulated. The results presented here are a continuation of a similar compilation[1] for hydrogen ions and neutrals in H_2.

The cross section data were assembled from published results. The choices of data for consideration were guided by their intended use in the modeling of electrical discharges in weakly ionized, low pressure N_2 and Ar. The data have been used in models of breakdown at high voltages and low pressures[2] in N_2 and Ar and in analyses of dc and transient emission measurements for low current, low pressure discharges[2–4] in N_2 and Ar. The data are also expected to be useful in models of the voltage–current characteristics[5,6] and ion fluxes[7] for the cathode fall of N_2 and Ar discharges at cathode-fall voltages[8] above 300 V and in analyses of the early stages of pseudo-spark discharges.[9] Studies utilizing similar data for the ions and neutrals[1] of H_2 have been used to analyze high voltage, low pressure breakdown,[8,10] ion sources,[11] and in "pseudo-spark" devices.[12] To the best of our knowledge there are no previous reviews that include recommended cross sections for nitrogen ions and neutrals in N_2 or of argon ions and neutrals in Ar at energies above thermal. This compilation supersedes our previous brief review.[13]

This paper is an effort to provide data of current need and is subject to revision as new data become available. The published cross sections have been interpolated and extrapolated where necessary to provide the "complete" sets of data needed for the models. We have not attempted to assign estimates of accuracy to the recommended data, but we have indicated areas of uncertainty and where extrapolations and interpolations were made. We have not considered gas mixtures or three-body collision processes. Collisions at near thermal energies of electronically excited states of N and N_2 with N_2 and of excited states of Ar with Ar are beyond the scope of this paper.

The cross sections and the transport and reaction coefficients for nitrogen ions and neutrals in N_2 are shown in Figs. 1–6 and are listed in Tables 1–6. The cross sections assembled from published experimental data for Ar^+ and Ar in Ar are shown in Figs. 7 and 9 and the associated tables, while transport and reaction coefficients are given in Figs. 8 and 10. The data and much of the discussion for Ar^+ in Ar and Ar in Ar are from an analysis of experiments by Phelps and Jelenković.[2]

Unless otherwise specified, all energies are laboratory energies ϵ_L rather than relative, center-of-mass, or "collision" energies. The same logarithmic energy scale is used in all of the cross section and energy loss tables because of the wide range of energies considered and the resultant simplicity of averages over the ion and fast neutral energy distributions. Although some entries in the tables are given to several significant figures, all entries should be considered uncertain to at least $\pm 5\%$. Blank entries in the tables indicate that the cross sections are too small to be evaluated, or are zero. In general, the curves and tables are labeled by the experimentally observed or theoretically calculated product of the collision.

2. Symbols

The symbols used in this paper are:

A	number of atoms in projectile
A'	number of atoms in target
e	electronic charge $= 1.602\times10^{-19}$ C
E/n	electric field to gas density ratio in Td
J	quantum number of rotational level of N_2 or N_2^+

$L_m(X)$ loss function for ion X in momentum balance model in eV m^2
M mass of projectile in atomic units
M' mass of target in atomic units
n gas density in molecules/m^3
n^* principal quantum number of N atom or N_2 molecule
Q_{CT} cross section for charge transfer collisions in m^2
$Q(e)$ total cross section for electron production in m^2
$Q(\lambda)$ total cross section for production of photons of wavelength λ in m^2
Q_d cross section for "destruction" or loss of ions or fast neutrals in m^2
Q_m momentum transfer cross section in m^2
$\bar{Q}(k)$ average cross section for process k in m^2
T_+ "temperature" characterizing energy distribution of N_2^+ ions in eV
Td unit of E/n such that 1 Td (townsend) $= 10^{-21}$ V m^2
v quantum number of vibrational level of N_2 or N_2^+ molecule
W_+ drift velocity of N_2^+ in N_2 or Ar^+ ions in Ar in m/s
W_m drift velocity of an ion calculated using momentum balance model in m/s
Z effective charge of projectile in units of electron charge
Z' effective charge of target in units of electron charge
$\alpha(k)$ spatial reaction or excitation coefficient for process k in m^{-1}
ΔJ change in rotational quantum number of N_2 or N_2^+
ϵ_L projectile energy in the laboratory frame in eV
$\langle\epsilon\rangle_i$ mean energy loss by projectile per ionizing collision in eV
ϵ_k energy loss in excitation of the k th level in eV
ϵ_m ion drift energy calculated using momentum balance model in eV
μn ion mobility normalized to unit density in (m V s)$^{-1}$

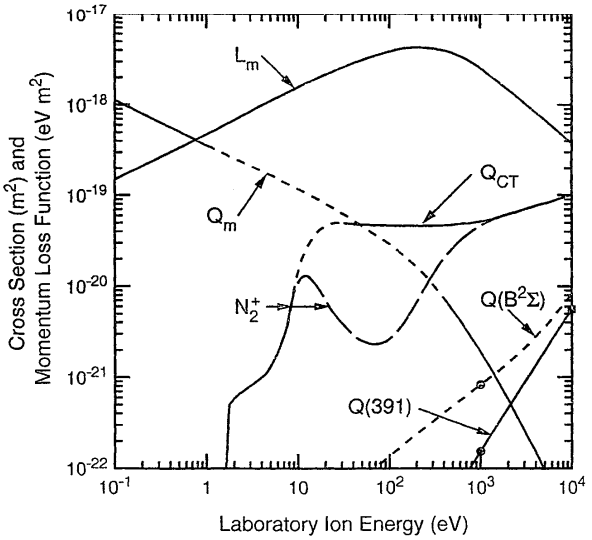

FIG. 1. Cross sections and momentum loss for collisions of N^+ with N_2 versus laboratory energy of N^+ for N_2 at rest. The symbols and collision processes are: Q_{CT} slow ion production by charge transfer; Q_m, momentum transfer; $Q(N_2^+)$, charge transfer to form N_2^+; $Q(B^2\Sigma)$, production of excited molecules emitting the N_2^+ $B^2\Sigma$ band system; and $Q(391)$, production of the N_2^+ 391.4-nm band. The curve labeled L_m is the momentum loss function calculated from these cross sections and appearing in the theory used to calculate the steady-state N^+ drift velocity and the nonequilibrium motion.

3. N^+ Collisions with N_2

3.1. N^+–N_2 Cross Sections

The momentum transfer cross sections Q_m shown in Fig. 1 and listed in Table 1 for $\epsilon_L < 1$ eV were adjusted to fit the mobility data given by Ellis *et al.*[14] for $E/n < 500$ Td using the momentum balance relations given in Ref. 1. These cross sections are about 30% larger than the cross sections calculated using the spiraling radius[15] and average polarizability from McDaniel and Mason.[16] Since the N^+–N_2 collision frequency is very nearly constant, the cross sections shown are in very good agreement with values obtained using the exact formulas[15] for thermal mobilities[14] and extrapolating to the energies shown.

The $Q_m(N^+,N_2)$ values shown for $500 < \epsilon_L < 1500$ eV are scaled from the $Q_m(H,H_2)$ values obtained previously[1] for H^+–H_2 collisions and for H–H_2 collisions using the relation

$$Q_m(X,X')/Q_m(H,H_2) = 2(M'+M)^2ZZ'AA'/9M^2, \quad (1)$$

where m and M are the masses of the projectile X and of the target X', Z, and Z' are the effective charges of the projectile and target, and A and A' are the number of atoms in the projectile and target molecule. The 9/2 factor is the combination of mass, charge, and number of atoms from Eq. (1) as applied to H^+–H_2 collisions. As in Ref. 1, this scaling is for fixed laboratory projectile energy and is adapted from the charge and mass dependence for screened Coulomb scattering[15] in which the atoms of the molecule are treated as independent scatterers and the change in screening length is neglected. The choice of $Z = Z' = 5$ in the present case is based on a comparison of differential scattering cross sections for H–H_2 collisions[17] relative to those for O–O collisions.[18] For O–O_2 collisions the use of $Z = Z' = 6$ in Eq. (1) works well, i.e., Z and Z' are determined by the number of electrons in the outer shell of the atom and the inner shell of electrons is not penetrated. The comparison is made for large products of energy and angle, i.e., $\gtrsim 20$ keV degree, where the scattering is approximately that for a Coulomb potential[17,19] and makes the dominant contribution[1] to Q_m. A limitation of this scaling should be noted in that for H–O_2 and H–N_2 collisions at large angles the use of Z' equal to the nuclear charge works better than the use of Z' equal to the number of electrons in the outer shell of the target. The Q_m values for N^+–N_2 shown by the short dashed curve of Fig. 1 are obtained by an arbitrary interpolation between the low and high energy Q_m values.

TABLE 1. Cross sections for $N^+ + N_2$ collisions by product. (Cross sections in units of 10^{-20} m^2.)

Lab. ion energy eV	Cross section $Q(N_2^+)$	$Q(391)$	$Q(B\,^2\Sigma)$	$Q(e)$	Q_m	L_m
0.1					112	14.9
0.133					97	17.2
0.1778					84	19.9
0.237					73	23.1
0.316					63	26.6
0.422					55	30.9
0.562					48	36.0
0.750					41.5	41.5
1					35.5	47.3
1.333					31.3	55.7
1.778	0.051				27	64.0
2.37	0.068				23.8	75.3
3.16	0.083				20.8	87.7
4.22	0.104				18	101.2
5.62	0.164				15.7	117.7
7.50	0.35				13.5	135.0
10	1.45				11.7	156.0
13.33	3				10	177.8
17.78	4.25				8.6	204
23.7	4.9				7.3	231
31.6	4.95		0.004	0.0	6.2	261
42.2	4.8		0.0063	0.0016	5.15	290
56.2	4.73		0.0085	0.0054	4.25	319
75.0	4.7		0.0109	0.0116	3.5	350
100	4.65		0.0137	0.0305	2.9	387
133.3	4.6		0.0172	0.077	2.3	409
177.8	4.6	0.000 93	0.0217	0.158	1.8	427
237	4.6	0.0015	0.0272	0.275	1.36	430
316	4.63	0.0025	0.0337	0.44	0.98	413
422	4.67	0.0039	0.0425	0.675	0.68	382
562	4.83	0.0061	0.053	0.97	0.46	345
750	4.95	0.0097	0.066	1.34	0.298	298
1000	5.17	0.0154	0.083	1.74	0.19	254
1333	5.44	0.0243	0.103	2.18	0.117	208
1778	6	0.038	0.13	2.74	0.07	166.4
2370	6.5	0.06	0.167	3.37	0.041	130.2
3160	7.1	0.094	0.218	4.06	0.0235	99.9
4220	7.8	0.148	0.297	4.9	0.0135	77.3
5620	8.4	0.233	0.407	5.87	0.0073	56.9
7500	9.25	0.365	0.58	6.93	0.0041	44.5
10 000	10.1	0.555	0.82	8.05	0.0024	37.7

The measurements of cross sections for charge transfer collisions of N^+ with N_2 fall into three types depending on which product is detected, i.e., slow ions, N_2^+, or fast N. The early measurements of N_2^+ production[20,21] have been extended by Maier and Murad.[22] At low ϵ_L collision complexes are formed and much of the available kinetic energy is converted into internal energy of the products. The N_2^+ production data are represented in Fig. 1 by the curve marked N_2^+ for $\epsilon_L < 200$ eV. Cross sections measured for slow ion production by Stebbings, Turner, and Smith[23] are shown by the curve marked Q_{CT}. Fast N atom production has been measured[24,25] for $\epsilon_L > 600$ eV and the cross sections are in general agreement with the results for slow ion production. Excited states of N^+ have been shown[25] to lead to larger cross sections for fast N production at $\epsilon_L > 1000$ eV, but this process has not been studied systematically at lower ϵ_L. The fact that cross sections for N_2^+ production[20–22] are consistently lower than those for slow ion and fast atom production[24,25] leads to the suggestion that the collection efficiency for N_2^+ is variable. This effect would account for the differences in the energy dependence of the derived N_2^+ production cross sections.[20–22] For our recommended cross section for the total production of N_2^+ and fast N, we have followed data of Stebbings, Turner, and Smith[23] for $30 < \epsilon_L < 5000$ eV and then extrapolated, as shown by the short dashed curve, to the low energy results of Maier and Murad.[22] Thus, we have assumed that the collection efficiency for N_2^+ approaches unity for $\epsilon_L < 10$ eV. Obviously, much additional work is necessary in order to obtain accurate cross sections at $\epsilon_L < 1$ keV.

We have found no information on rotational or vibrational excitation of ground state N_2 in N^+–N_2 collisions. As appears to be the case[1] for rotational excitation in H^+–H_2, we expect the long range charge-quadrupole interaction to cause the $\Delta J = 2$ cross sections to rise rapidly with ϵ_L at energies just above the various thresholds for the rotational

levels of the thermally excited N_2 molecules.

Cross sections are shown in Fig. 1 and listed in Table 1 for excitation of the $B\,^2\Sigma_u^+$ state of N_2^+ and for excitation of the 391.5-nm band emitted in the $B\,^2\Sigma$–$X\,^2\Sigma$, $v' = 0$ to $v'' = 0$ transition. The only measurements of the cross sections for $\epsilon_L \leqslant 10$ keV are those of Ottinger and Simonis[26] (solid circles) at 1 keV and that of Sheridan and Clark[27] (solid square) for the 391.4-nm band at 10 keV. The recommended cross sections shown by the short dashed lines drawn through the points take into account the relative increase of excitation of the higher vibrational levels with decreasing ϵ_L found in experiment.[28,29] Excitation of the $C\,^3\Pi_u$ state leading to emission of the 2nd positive band was negligible in most experiments[26] and when observed was attributed to excitation by secondary electrons.[28] The cross section for excitation of the ^3P–^1S transition for N^+ has been observed by Moore[30] to be $\approx 10^{-24}$ m^2 for $\epsilon_L \approx 1$ keV.

There is very little information available regarding electron production in N^+–N_2 collisions. We have taken the electron production cross section $Q(e)$ to be equal to that for ionization in N_2–N_2 collisions from Sec. 5.1. Note that we have not included the low energy electron production (ionization) process proposed by Maier and Murad[22] to increase sharply at $\epsilon_L \approx 35$ eV.

3.2. Drift Velocities and Reaction Coefficients for N^+ in N_2

The drift velocities of N^+ in N_2 calculated using the cross sections of Fig. 1 and Table 1 are shown by the solid curve of Fig. 2 labeled W_m where they are plotted as a function of the electric field to gas density ratio E/n. As discussed in Sec. 3.1, the momentum transfer cross section Q_m at low ϵ_L has been adjusted to fit the experimental drift velocity data from Ellis *et al.*[14] for $E/n < 500$ Td, where 1 Td $= 10^{-21}$ V m^2. The simplified momentum balance theory used for these drift velocity calculations is discussed in detail in Ref. 1. In steady-state limit, this simple model balances the momentum loss by a monoenergetic beam of H^+ in collisions with H_2 against the momentum gain from the electric field. The momentum loss function L_m needed for this calculation is derived from the cross section set of Fig. 1 and is shown in the uppermost curve of Fig. 1 and is listed in Table 1. At E/n near 4.3×10^3 Td the calculated drift velocity becomes indeterminate because of the phenomenon of "runaway" in which the energy that the N^+ ions gain from the electric field is no longer balanced by the energy lost to collisions with N_2. The tabulated drift velocities are given in Table 2.

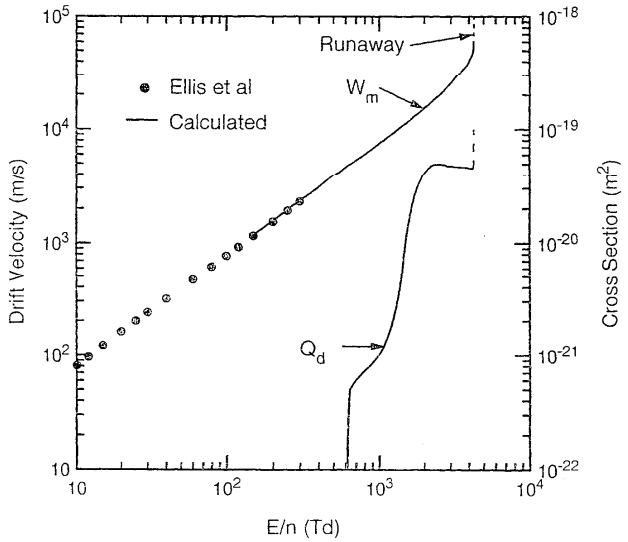

FIG. 2. Drift velocities W_m and effective destruction cross section Q_d for N^+ in N_2 versus E/n. The points are experimental data from Ellis *et al.*[14] The smooth curves are calculated from the momentum balance theory.

TABLE 2. Calculated drift velocities and cross sections versus E/n for N^+ in N_2. (The cross sections are in units of 10^{-20} m^2.)

E/n Td	W_m m/s	T_+ eV	$Q_d(N^+)$	$Q(391)$	$Q(e)$
149	1173	0.1			
199	1564	0.1778			
265	2090	0.316			
359	2780	0.562			
473	3710	1			
640	4950	1.778	0.051		
877	6600	3.16	0.083		
1177	8800	5.62	0.164		
1559	11 730	10	1.45		
2040	15 650	17.78	4.25		
2610	20 870	31.6	4.95		0.004
3190	27 830	56.2	4.73		0.0085
3870	37 100	100	4.65		0.0137
4270	49 500	177.8	4.6	0.000 93	0.0217
4300	57 100	237	4.6	0.0015	0.0272

Figure 2 shows the total cross section for N^+ destruction Q_d. In the energy range of interest we assumed $Q_d = Q_{CT}$. Table 2 also lists cross sections for excitation of the 391.4-nm band of N_2 $Q(391)$ and electron production $Q(e)$ for N^+ in N_2. Because of the simplicity of our momentum balance model,[1] the values shown in Fig. 1 and Table 2 are the cross sections from Fig. 1 evaluated at the energy of the drifting N^+. We note that measurements of the N^+ drift velocity are not reported for E/n for which the destruction is significant, although it is not clear that the calculated Q_d values are large enough to account for the apparent loss of N^+ signal for $600 < E/n < 1000$ Td. In applying the cross section data of Table 2, one must keep in mind that calculations using more accurate steady-state ion energy distributions would result in a smearing out of the spatial reaction coefficient versus E/n relative to the cross sections versus E/n of Fig. 2 and Table 2.

4. N_2^+ Collisions with N_2

4.1. N_2^+–N_2 Cross Sections

The charge transfer section Q_{CT} for N_2^+ collisions with N_2 shown in Fig. 3 and tabulated in Table 3 at $\epsilon_L \approx 1$ eV is adjusted to fit the measurements of N_2^+ drift velocity[14] as discussed in Sec. 4.2. A smooth extrapolation to these Q_{CT} values from higher ϵ_L leads us to recommend the results of Stebbings, Turner, and Smith[23] and Kobayashi[31] from

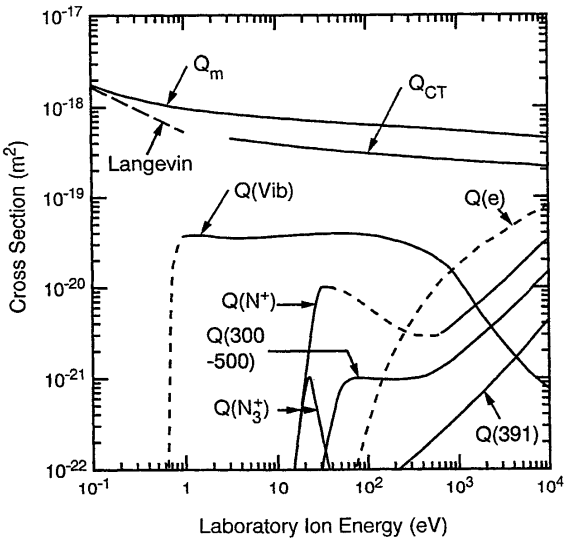

FIG. 3. Cross sections for collisions of N_2^+ with N_2 versus laboratory energy of N_2^+ for N_2 at rest. The symbols and collision processes are: Q_m, momentum transfer; Q_{CT}, charge transfer; Q(Vib.), vibrational excitation; $Q(N^+)$, formation of N^+; $Q(N_3^+)$, production of N_3^+; $Q(e)$, electron production; Q(300–500), production of radiation in the range from 300 to 500 nm; Q(391), production of the 391.4-nm band of N_2^+. The short dashed portions of the curves indicate a higher degree of uncertainty in the recommended cross section.

among the many measurements of the charge transfer cross section. The charge transfer cross section Q_{CT} is not shown or tabulated for $\epsilon_L < 1$ eV because the approach to isotropic scattering instead of the 180° scattering in the center-of-mass frame makes the concept of charge transfer questionable. The cross section for momentum transfer collisions Q_m for N_2^+ with N_2 shown in Fig. 3 and tabulated in Table 3 is chosen to approach the spiraling or "Langevin" cross section for polarization scattering[15,16] at low ϵ_L and twice[16,32] the charge transfer cross section Q_{CT} at high ϵ_L. Through measurements of differential scattering, Friedrich *et al.*[33] have shown the importance of collision complex formation and translational to internal energy exchange at $\epsilon_L = 1.5$ eV and of the traditional electron-hopping mechanism at $\epsilon_L = 20$ eV.

We have found no data on rotational excitation in N_2^+–N_2 collisions at low ϵ_L, but expect that as for H^+–H_2 collisions the charge-quadrupole interaction will lead to a significant cross section near the various thresholds. At $\epsilon_L = 800$ eV, Ding and Richter[34] find that N_2^+–N_2 collisions result in significant rotational excitation of the fast N_2^+ but not of the slow N_2^+ produced by charge transfer. Because of the lack of quantitative data, we have made no recommendation for rotational excitation in Fig. 3 or Table 3.

The vibrational excitation cross section Q(Vib) shown in Fig. 3 and listed in Table 3 is the sum of the vibrational cross sections given by Moran, McCann, and Flannery.[35] The cross sections for $\Delta v = 1$ excitation of the N_2^+ and N_2 are comparable at energies up to 2 keV. The $\Delta v = 2$ contribution to the sum decreases from about 30% at energies just above threshold to a very small fraction at 2 keV. Ding and Richter[34] find that at $\epsilon_L = 800$ eV there is a significant production of vibrationally excited slow N_2^+ in charge transfer collisions and little vibrational excitation for the fast N_2^+. Unfortunately, they do not extract relative rotationally inelastic, charge transfer, and vibrational excitation cross sections and so do not test the theory shown in Fig. 3. In contrast, McAfee *et al.*[36] find experimental and theoretical evidence for "efficient" vibrational excitation of Δv up to 4 for forward scattering N_2^+ at $\epsilon_L = 111$ eV. The rate coefficient for vibrational deexcitation of N_2^+ by N_2 at 300 K has been measured[37] to be about 60% of the Langevin value. Application of detailed balancing[1,38] and extrapolation of this result to energies of a fraction of an electron volt yield excitation cross sections that are roughly equal to predictions of the theory shown in Fig. 3.

The cross section for formation of N^+ in N_2^+ ($X\,^2\Sigma$)–N_2 collisions shown in Fig. 3 is based on the data of Maier[39] for $\epsilon_L < 45$ eV and that of Moran, Wilcox, and Abbey[40] for $650 < \epsilon_L < 5$ keV. The apparent cross sections vary with the energy of the electrons used to produce the N_2^+ because of the presence of long-lived excited electronic and vibrational states in the N_2^+ beam.[39,40] The data shown are for electron energies less than the experimentally observed threshold of 22–24 eV so as to eliminate[39] the electronically excited state component of the N_2^+ beam, e.g., that component responsible for N^+ production at $\epsilon_L < 15$ eV. One of the referees has suggested that the large change in the apparent cross section between 45 and 650 eV results from a change in the fraction of fast N^+ with ϵ_L caused by the decreasing importance of complex intermediates.[39] Measurements of the angular distributions of the products are not available to verify this suggestion. Moran, Wilcox, and Abbey[40] give cross sections for N^+ production from N_2^+ in $A\,^2\Pi(v)$ state which vary from 3.5 and 1.1 times the values shown in Fig. 3 as ϵ_L increases from 650 eV to 5 keV. There is very little quantitative information regarding the cross section for N^+ production in $A\,^2\Pi(v)$–N_2 collisions at lower values of ϵ_L. Maier[39] finds that the apparent cross section for N^+ production from an unidentified excited N_2^+ state, possibly the $A\,^2\Pi(v)$ state, increases with increasing ϵ_L at $\epsilon_L < 15$ eV, but does not give the magnitude. Also, he does not attempt separation of the excited state contribution at higher energies. The very large cross section for N^+ formation found by Leventhal and Friedman[41] is very difficult to reconcile with the more recent measurements.[39,40]

The cross section for formation of N_3^+ in ground state N_2^+–N_2 collisions shown in Fig. 3 is from Maier.[39] Several experimenters[39,42,43] obtained evidence that N_3^+ production at $\epsilon_L < 10$ eV is caused by N_2^+ in an unidentified, long-lived excited state. The apparent cross section for formation of N_3^+ from excited N_2^+ increases with decreasing ϵ_L. Most experiments[42,43] find that the threshold for production of this excited state by electrons is near 21 eV. Again the experiments of Leventhal and Friedman[41] are very difficult to reconcile with the later experiments.[39]

The excitation cross sections for the N_2^+ $B \rightarrow X$ (0,0), first-negative band at 391.4 nm presented in Fig. 3 and Table 3 are an average of the experimental data.[44–46] The cross sections for excitation of emission at wavelengths between

TABLE 3. Cross sections for $N_2^+ + N_2$ collisions by product. (Cross sections in units of 10^{-20} m^2.)

Lab. ion energy eV	Cross section Q(Vib) (0.29)[a]	Q_{CT}	$Q(N^+)$ (15)	$Q(N_2^+)$ (15)	Q(391) (18.8)	Q(300–500) (18.8)	Q_m	L_m
0.1							177	14.3
0.1333							159	17.20
0.1778							143	21.0
0.237							132	25.8
0.316							123	32.2
0.422							114	40.0
0.562							107.5	50.6
0.750	1.75						101	63.9
1	3.7						96.5	82.1
1.334	3.8						92.5	104.6
1.778	3.73						89.3	134.1
2.37	3.6						86	173.7
3.16	3.53	45					84	225
4.22	3.52	43.3					81.3	289
5.62	3.55	41.6					79.3	379
7.50	3.62	40.5					77.5	491
10	3.7	38.7					75.5	635
13.34	3.74	37.5	0.0034	0.0034			74	820
17.78	3.82	36	0.037	0.035			72	1079
23.7	3.87	35	0.31	0.09			70	1400
31.6	3.92	34	1.01	0.0215		0.0122	69	1823
42.2	3.95	33	0.99	0.0042		0.042	67.5	2390
56.2	3.95	32	0.89			0.0895	66	3100
75.0	3.9	31.3	0.75			0.101	64.5	4050
100	3.8	30.6	0.61		0	0.1	63.3	5240
133.4	3.65	29.7	0.49		0.007	0.098	62.3	6830
177.8	3.4	29	0.40		0.008	0.097	60.7	8930
237	3.16	28.3	0.34		0.0107	0.097	60	11 630
316	2.85	27.7	0.30		0.0137	0.1	58.7	15 190
422	2.5	27	0.29		0.0175	0.1045	57.5	19 830
562	2.14	26.3	0.29		0.0227	0.12	56.3	25 900
750	1.72	26	0.34		0.0295	0.143	55	33 600
1000	1.22	25.4	0.435		0.0387	0.18	54	44 000
1334	0.8	24.8	0.55		0.051	0.228	52.7	57 700
1778	0.51	24.2	0.695		0.067	0.292	51.3	74 700
2370	0.345	23.8	0.90		0.091	0.374	50	97 800
3160	0.238	23.3	1.16		0.123	0.484	49	127 800
4220	0.17	22.9	1.53		0.165	0.635	47.7	167 100
5620	0.124	22.7	2.00		0.227	0.83	46.7	217 000
7500	0.095	22	2.64		0.317	1.13	45.7	288 000
10 000	0.076	21.4	3.4		0.44	1.48	44.6	372 000

[a] The numbers in parentheses are the threshold energies in the center-of-mass frame.

300 and 500 nm are from measurements by Liu and Broida[46] after renormalization to the scale used for the 391.4 nm emission. About 80% of this emission appears to be from the $v = 0$ level of the $B\,^2\Sigma_u^+$ state of N_2^+ with the excitation shifting to higher vibrational levels of the B state as ϵ_L decreases.[45,46] This shift is similar to that observed for N^+–N_2 collisions. The cross sections for emission by lines of NII at wavelengths near 500 nm is observed[45] to be about 5% of that due to the first-negative system and is not shown or listed.

We have found no information on the production of electrons and either N^+ or N_2^+ ions in N_2^+–N_2 collisions, and so have adopted the cross section for N_2–N_2 collisions[17] from Sec. 5.1. This cross section is shown by the short dashed line, where the short dashes indicate a high degree of uncertainty.

4.2. Transport and Reaction Coefficients for N_2^+ in N_2

Figure 4 and Table 4 give the drift velocities and reaction coefficients for N_2^+ in N_2 calculated from the cross sections of Sec. 4.1 using the theory outlined in Ref. 1. Because of the large values of the charge exchange and momentum transfer cross sections for N_2^+ in N_2, it is often a good approximation to assume that in drift tube experiments the N_2^+ ions are in equilibrium with the applied field, i.e., that the energy gained from the field is balanced by energy lost in collisions. We have therefore calculated the drift velocities W_+, the ion "temperature" T_+, and the reaction coefficients assuming that the energy distribution of the ions is the equilibrium distribution at the applied E/n value.[1,15,48] As indicated in Sec. 4.1 we have chosen charge transfer cross section values such that the calculated drift velocities are in good

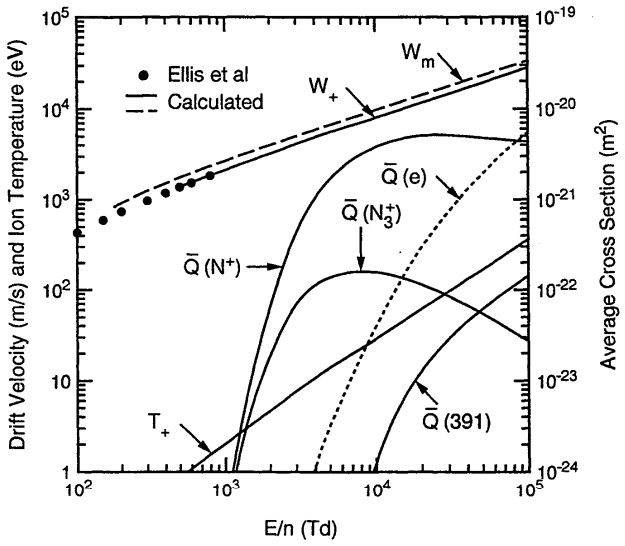

FIG. 4. Drift velocities W_+ and W_m, ion "temperature" T_+, and average cross sections Q are shown as a function of E/n for N_2^+ drifting through N_2. The points are experimental data from Ellis *et al.*[14] The average cross sections are calculated from the cross sections of Fig. 3 using theoretical equilibrium energy distributions for N_2^+ in N_2.

agreement with the experimental values from Ellis *et al.*[14] Thus, the solid curve labeled W_+ in Fig. 4 was calculated from the Q_{CT} values of Fig. 3 using Eq. (7) of Ref. 1. We note that the drift velocities W_m calculated using the momentum transfer cross sections Q_m of Fig. 3 and shown by the dashed curve are in rather good agreement with experiment and with calculations of W_+ using Q_{CT}. The calculated values of the ion "temperature" T_+ which characterize the one-dimensional energy distribution of the N_2^+ ion in N_2 are shown in Fig. 4. Since the velocity distribution of the ions is one dimensional, the average ion energy is equal to $kT_+/2$. We know of no experimental data with which to make a comparison of ion energies.

Evidence for rotational excitation of N_2^+ in N_2^+–N_2 collisions under swarm conditions has been obtained by Borysow and Phelps.[49] At $E/n = 110$ Td they find an increase in the N_2^+ rotational temperature of 60 K above the gas temperature of 300 K. As yet, no cross section information has been derived from the data.

We know of no experimental vibrational excitation coefficient data for N_2^+ in N_2^+–N_2 collisions under swarm conditions, although rate coefficients have been measured for N_2^+–N_2 deexcitation collisions[37] as discussed in Sec. 4.1.

Figure 4 and Table 4 show the calculated spatial reaction coefficients or average cross sections $\bar{Q}(N^+)$ for the dissociation of N_2^+ to form N^+ and $\bar{Q}(N_3^+)$ for the reaction to form N_3^+ as a function of E/n. As discussed in Ref. 1, when charge transfer collisions dominate, the reaction coefficients are equal to the averages of the corresponding cross sections over the ion energy distribution. We take advantage of this special situation to use the compact notation $\bar{Q}$ for the average cross section, rather than the conventional and more cumbersome notation of α/n for the spatial reaction coefficient.[2,3]

Applications of the average cross sections of Fig. 4 are subject to the considerable uncertainties regarding the excited state of the incident N_2^+ ion discussed in Sec. 4.1. The only swarm experiment reporting the apparent dissociation of N_2^+ to form N^+ is that of Fletcher and Blevin.[50] An explanation of this experiment in terms of collisional dissociation of N_2^+ would require an average cross section $\bar{Q}(N^+)$ that is $\approx 10^{-21}$ m^2 at E/n near 700 Td and which increases rapidly with E/n. This value is many orders of magnitude larger than that obtained by the calculations shown in Fig. 4 and Table 4. It remains to be seen whether models will predict a sufficient population of the as yet unidentified excited states of N_2^+ to explain these results.

The average cross section for the production of electrons $\bar{Q}(e)$ in Fig. 4 is shown as a short dashed curve to emphasize the uncertainty in this coefficient resulting from the use of the measured ionization cross section for N_2–N_2 collisions in the absence of data for electron production in N_2^+–N_2 collisions. The calculated reaction coefficient for the excitation of 391.4 nm emission in N_2^+–N_2 collisions is quite small and generally results in negligible excitation compared to that produced by electron excitation.[3]

Note that mass spectrometer and drift tube experiments are more sensitive to ion–molecule reactions involving excited states than are the beam experiments of Sec. 4.1 because

TABLE 4. Calculated transport coefficients and average cross sections for N_2^+ in N_2.

E/n Td	Q_m m^2	T_+ eV	W_+ m/s	$\bar{Q}(N^+)$ m^2	$\bar{Q}$(391 nm) m^2	$\bar{Q}(N_3^+)$ m^2	$\bar{Q}(e)$ m^2
500	5.70E–19[a]	0.877	1387	4.06E–29	...[b]	4.04E–29	...
1000	4.90E–19	2.04	2120	3.47E–25	...	2.65E–25	1.10E–31
2000	4.30E–19	4.65	3190	6.35E–23	2.04E–34	1.86E–23	5.95E–27
3000	3.90E–19	7.69	4110	4.28E–22	1.34E–29	6.91E–23	2.21E–25
5000	3.60E–19	13.89	5520	1.66E–21	1.39E–26	1.36E–22	3.20E–24
10 000	3.48E–19	28.7	7940	3.78E–21	1.27E–24	1.57E–22	3.91E–23
20 000	3.24E–19	61.7	11 640	5.07E–21	1.29E–23	1.14E–22	2.96E–22
50 000	3.00E–19	166.7	19 100	4.80E–21	6.14E–23	5.45E–23	1.92E–21
100 000	2.76E–19	362	28 200	4.33E–21	1.42E–22	2.72E–23	5.46E–21

[a] 5.70E–19 means 5.70×10^{-19}.
[b] Too small for accurate calculation.

the higher gas densities and shorter time delays between production of the excited ion and collisions with N_2 increase the probability of reaction relative to radiation. In addition, the generally lower values of ϵ_L in mass spectrometers and drift tubes mean that they are especially sensitive to excited state processes.

5. N_3^+ and N_4^+ Collisions with N_2

The only data we have found on collisions of N_3^+ with N_2 are measurements of the drift velocity[14] of N_3^+ in N_2 for $2 < E/n < 240$ Td, corresponding to ion energies up to 0.7 eV. The momentum transfer cross section required to fit the drift velocity data is about 40% larger than that for N^+ collisions with N_2. At $\epsilon_L > 500$ eV scaling factor given by Eq. (1) results in a predicted cross section for N_3^+ with N_2 which is ≈ 8 times that for N^+ with N_2. In view of the accumulating uncertainties, we have not shown or tabulated these estimates of Q_m. The situation is even worse for the potentially important reaction of dissociation of N_3^+ in collisions with N_2. Here the drift tube experiments yield no evidence[51,52] for dissociation for $E/n < 100$ Td and some evidence[52] for dissociation from the anomalous behavior of the ion current waveforms for $E/n > 300$ Td. Discussion of the data[43,51–55] regarding the formation of N_3^+ in three-body collisions of N^+ with N_2 is outside the scope of this paper.

All of the data we have found on collisions of N_4^+ with N_2 are from measurements in drift tubes for $10 < E/n < 200$ Td, corresponding to ion energies up to 0.6 eV. The momentum transfer cross section required to fit the drift velocity data[54] is about 10% larger than that for N^+ collisions with N_2. At $\epsilon_L > 500$ eV the scaling factor given by Eq. (1) results in a predicted cross section for N_3^+ with N_2 which is ≈ 16 times that for N^+ with N_2. In view of the accumulating uncertainties, we have not shown or tabulated the estimates of Q_m. Drift tube experiments yield dissociation rate coefficients increasing from $\approx 10^{-19}$ m^3/s for $E/n = 100$ Td to $\approx 10^{-17}$ m^3/s for $E/n = 200$ Td. Discussion of the data[53,55] regarding the formation of N_4^+ in three-body collisions of N_2^+ with N_2 and of the N_2^+–N_2 bond energy is outside the scope of this paper.

6. N Collisions with N_2

Since there are no data on which to base estimates of the momentum transfer cross sections Q_m for N with N_2, we recommend that one use 60% of the values for $N_2 + N_2$ collisions. This scaling factor is approximately that found[1] for $H + H_2$ collisions as compared to $H_2 + H_2$ collisions and is consistent with the scaling factor given by Eq. (1).

Vibrational deexcitation in N–N_2 collisions has been investigated theoretically by Laganà, Garcia, and Ciccarelli.[56] They find that the cross sections are very small except for very high initial vibrational states. We have not shown or tabulated their results.

7. N_2 Collisions with N_2

7.1. N_2–N_2 Cross Sections

The momentum transfer cross sections Q_m shown in Fig. 5 and listed in Table 5 for $\epsilon_L < 1$ eV were calculated from temperature dependent diffusion coefficient measurements[57] as outlined in Ref. 1. The Q_m values for $\epsilon_L > 500$ eV were scaled from $Q_m(H,H_2)$ and $Q_m(O,O_2)$ values using Eq. (1) as described in Sec. 3.1.

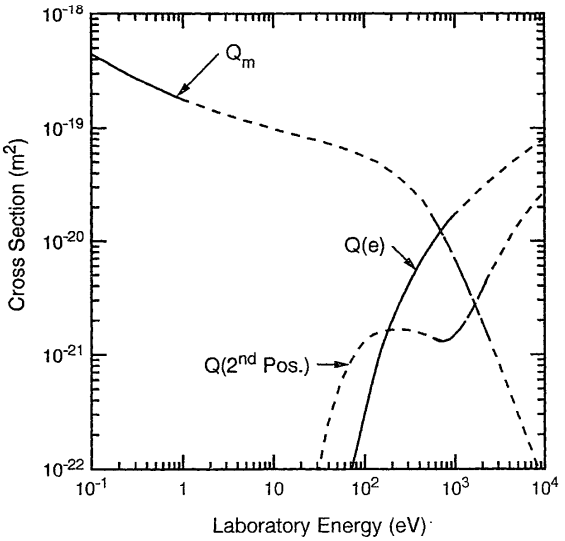

FIG. 5. Cross sections for collisions for N_2 with N_2 versus laboratory energy of the projectile N_2 for the target N_2 at rest. The symbols and associated cross sections are: Q_m, momentum transfer; $Q(e)$, electron production; and Q(2nd Pos.), production of the 2nd positive system of N_2. The shorter dashes indicate a greater uncertainty in the cross section.

Vibrational excitation and deexcitation in N_2–N_2 collisions has been observed experimentally[58] to have very small rate coefficients for gas temperatures below 6000 K. Although we have not done so, the procedures of Ref. 1 could be used to derive the vibrational excitation cross section at energies near threshold. The available theory[59] appears to be limited to the same energy range as the experiments.

The energy dependence of the cross section for excitation of the 406 nm band of the $C\,^3\Pi_u \rightarrow B\,^3\Pi_g$ 2nd positive system of N_2 for $500 < \epsilon_L < 200$ eV shown in Fig. 5 is from Sheridan and Peterson.[60] The magnitude corresponds roughly to that required to fit the drift tube data of Jelenković and Phelps[3] for the 337-nm band of the 2nd positive system. Note that the 337 and 406-nm bands have the same upper vibrational state, i.e., $v' = 0$. We have therefore labeled the cross section Q (2nd Pos.). The cross section has been extended to lower ϵ_L as indicated by the short dashed curve so as to approach zero at the expected excitation threshold.

Cross sections for negative charge production, i.e., electron production, in N_2–N_2 collisions from Utterback and Van Zyl[17] are shown in Fig. 5 and Table 5.

7.2. N_2–N_2 Average Cross Sections

Since the fast N_2 molecules found in drift tube and electrical discharges are usually produced by charge transfer collisions of N_2^+ with N_2, the fast N_2 has an initial energy distribution which is the same as the equilibrium N_2^+. We therefore find it convenient to describe the reactions of N_2 with N_2 in terms of reaction coefficients or average cross

TABLE 5. Cross sections for $N_2 + N_2$ collisions tabulated by product. (Cross sections in units of 10^{-20} m^2.)

Lab. molecule energy eV	Cross section $Q(2^{nd}$ Pos.) (18)[a]	$Q(e)$ (15.6)	Q_m
0.1			44.5
0.1333			39.2
0.1778			34.3
0.237			30.2
0.316			26.8
0.422			24.2
0.562			21.8
0.750			19.7
1			17.9
1.334			16.6
1.778			15.2
2.37			14
3.16			13
4.22			12.1
5.62			11.3
7.50			10.6
10			9.8
13.34			9.25
17.78			8.7
23.7	0.0		8.2
31.6	0.01	0.0	7.75
42.2	0.03	0.0016	7.25
56.2	0.06	0.0054	6.75
75.0	0.0955	0.0116	6.23
100	0.131	0.0305	5.6
133.4	0.153	0.077	5.03
177.8	0.163	0.158	4.33
237	0.167	0.275	3.65
316	0.162	0.44	2.93
422	0.153	0.675	2.35
562	0.14	0.97	1.63
750	0.131	1.34	1.08
1000	0.151	1.74	0.68
1334	0.203	2.18	0.405
1778	0.31	2.74	0.237
2370	0.5	3.37	0.137
3160	0.75	4.06	0.077
4220	1.13	4.9	0.043
5620	1.58	5.87	0.0235
7500	2.13	6.93	0.013
10 000	2.72	8.05	0.0072

[a] The numbers in parentheses are the threshold energies in the center-of-mass frame.

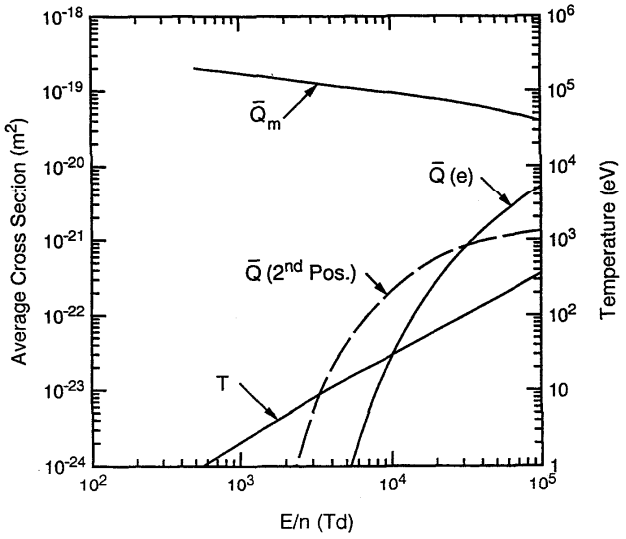

FIG. 6. Reaction coefficients or average cross sections as a function of E/n for N_2 formed by charge transfer collisions from N_2^+ drifting through N_2. The curves show the average cross sections for momentum transfer $\bar{Q}_m$, of electron production $\bar{Q}(e)$, and for production of 2nd positive system of N_2 $\bar{Q}$(2nd Pos.). The latter curve is only roughly normalized to swarm experiment. The curve labeled T is from Fig. 4 and shows the theoretical temperature of the N_2 formed from charge transfer collision between N_2^+ and N_2.

TABLE 6. Reaction coefficients for $N_2 + N_2$ collisions.

E/n Td	T eV	$\bar{Q}$(2nd Pos.) m^2	$\bar{Q}(e)$ m^2	$\bar{Q}_m$ m^2
500	0.877	...[b]	...	2.03E-19[b]
1000	2.04	...	...	1.73E-19
2000	4.65	3.21E-25	...	1.44E-19
3000	7.69	4.92E-24	2.70E-27	1.28E-19
5000	13.89	4.06E-23	6.33E-25	1.11E-19
10 000	28.7	2.08E-22	2.71E-23	9.39E-20
20 000	61.7	5.65E-22	2.78E-22	7.75E-20
50 000	166.7	1.06E-21	1.91E-21	5.63E-20
100 000	362	1.32E-21	5.43E-21	3.98E-20

[a] Too small for meaningful calculation.
[b] 2.03E-19 means $2.03 \cdot 10^{-19}$.

sections as a function of the E/n which determines the N_2^+ in N_2 energy distribution. The average cross sections for collisions of N_2 with N_2, calculated using the cross sections of Fig. 5 and Table 5, are shown in Fig. 6 and listed in Table 6.

The average cross section for momentum transfer collisions $\bar{Q}_m$ shown in Fig. 5 is useful in modeling because it is the probability per unit distance at unit gas density that a N_2 molecule will lose a large fraction of its kinetic energy and so, in many situations, become incapable of excitation or ionization. The average cross section for the 2nd band system of N_2 $\bar{Q}$(2nd Pos.) shown in Fig. 6 is calculated from the Q(2nd Pos.) values of Fig. 5. The lower E/n portion of the curve is shown as short dashes because of the necessity for extrapolation of the corresponding cross section to low ϵ_L.

The average cross sections for electron production for N_2–N_2 collisions shown in Fig. 6 are calculated from the experimental cross sections.[47]

8. Ar^+ Collisions with Ar

8.1. Ar^+–Ar Cross Sections

The cross section sets that we have assembled from the literature for Ar^+ collisions with Ar are shown in Fig. 7 and are tabulated in Table 7. In Fig. 7 the charge transfer cross section Q_{CT} for Ar^+ with Ar at low energies is from Hegerberg, Elford, and Skullerud,[61] where agreement with transport data is more important to use than is agreement with beam data.[15,62] At higher energies we have used an average of the somewhat scattered experimental and theoretical results as given by McDaniel.[15] The cross section for momentum transfer collisions Q_m for Ar^+ with Ar shown in Fig. 7 and tabulated in Table 7 is chosen to approach the spiraling or "Langevin" cross section for polarization scattering[15,16] at low ϵ_L and twice[16,31] the charge transfer cross section Q_{CT} at high ϵ_L.

Note added in proof. Recent modeling of ion fluxes extracted from plasma processing discharges shows the importance of large-angle differential scattering data for Ar^+–Ar collisions [see Thompson, Sawin, and Fisher, J. Appl. Phys. **63**, 2241 (1988)]. Such absolute measurements have been made by Aberth and Lorents [Phys. Rev. **144**, 109 (1966)] and Vestal, Blakely, and Futrell [Phys. Rev. A **17**, 1337 (1978)]. We thank H. H. Sawin for pointing out the latter reference. Note that these two sets of differential scattering cross sections differ by about a factor of 2 in magnitude and 2 eV in energy. The charge transfer cross sections derived from the differential scattering data by Vestal, Blakely, and Futrell average to about 60% of the values recommended in Fig. 7 and Table 7. We recommend the use of their energy scale and that their magnitudes be increased by a factor of 1.6. The data of Aberth and Lorents would then be shifted up in energy by 2 eV and multiplied in magnitude by a factor of 0.8. It appears to be the more useful at low angles.

Figure 7 also shows cross sections for excitation of the UV radiation Q(UV) emitted by the resonance states of Ar. The sum of the cross sections shown for excitation of the resonance lines of Ar by Ar^+ are from the unpublished results of Isler and Murray.[63] Excitation of metastable Ar in

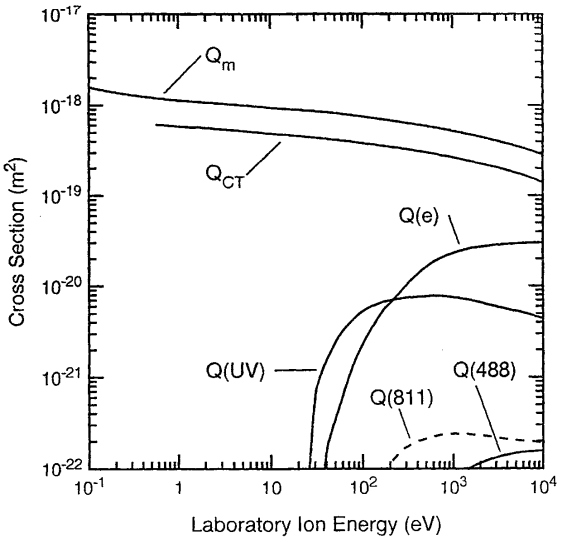

FIG. 7. Cross sections for Ar^+–Ar collisions versus laboratory energy. The symbols and collision process: Q_{CT}, charge transfer; Q_m, momentum transfer: $Q(e)$, production of electrons; Q(488), ArII 488-nm line excitation; Q(UV), ArI UV resonance line excitation; and Q(811), ArI 811-nm excitation. The cross section for excitation of the Ar lines near 811 nm is estimated from the Ne 614.3-nm line excitation in Ne^+–Ne collisions.

Ar^+–Ar collisions has been observed only at energies below 50 eV,[64] but the derived cross sections are too small to show in Fig. 7. These cross sections are much smaller than one would expect if the curve crossing model[65] used to describe resonance state excitation by Ar^+ also applies to the metastable states of the Ar $1s_n$ configuration (Paschen notation[66]). We suggest the cross sections for resonance line production Q(UV) as an upper limit to cross sections for metastable production.

The strongest lines in the near visible emission spectrum are expected to be those between the $2p_n$ and $2s_n$ levels (Paschen notation[66]). These lines, especially the lines near 811 nm, are easily observed in drift tube experiments[67] and the question arises as to whether they are excited in Ar^+–Ar collisions. We find no references to emission from these transitions as the result of Ar^+–Ar collisions.[67,68] We will assume that the 811-nm excitation cross section Q(811) for Ar^+ on Ar is equal to the cross sections for excitation in Ne^+–Ne collisions of the corresponding Ne transition,[66] i.e., the 640.2-nm line. At 2.5 keV the measured[63] 640.2-nm cross section is within 10% of the cross section for excitation of the 614.3-nm line of Ne by Ne^+. We will assume these two Ne excitation cross sections to be equal at all energies, so that Q(811) equals the measured cross section[63] for the Ne 614.3-nm line.

The cross section for excitation of the 488-nm line of ArII Q(488) is from Isler.[63]

The electron production or ionization cross section for Ar^+ on Ar $Q(e)$ is from Stuyters *et al.*[70]

TABLE 7. Cross sections for $Ar^+ + Ar$ tabulated by product.

Lab. ion energy eV	Product Q_{CT}	$Q(e)$ (15.8)[a]	Q(UV) (11.8)	Q(488) (22)	Q(811) (13.1)	Q_m
0.1						157
0.133 352						148
0.177 827						142
0.237 137						134
0.316 227						128
0.421 696						124
0.562 341	61					120
0.749 894	60					116
1	58.5					113
1.333 521	57.3					110
1.778 279	57					108
2.371 373	55.5					106.5
3.162 277	54					104
4.216 965	53					102.5
5.623 413	51.5					101
7.498 942	50					98.5
10	48.7					94.2
13.335 21	47.7					92.5
17.782 79	46.3					90.5
23.713 73	45		0.002			88
31.622 77	43.7	0.001	0.08			85.7
42.169 65	42.3	0.02	0.17			83
56.234 13	41	0.05	0.29			80.5
74.989 42	39.7	0.12	0.41		0.0012	77.5
100	38	0.23	0.53	0.000 07	0.003	75
133.3521	36.9	0.38	0.615	0.000 16	0.0059	72
177.8279	35.3	0.58	0.68	0.000 39	0.0097	69
237.1373	34	0.78	0.72	0.000 83	0.014	66.5
316.2277	32.6	1.07	0.75	0.001 56	0.0177	63.5
421.6965	31	1.4	0.76	0.002 68	0.0202	60.3
562.3413	29.7	1.75	0.775	0.0041	0.022	57.7
749.8942	28	2.05	0.775	0.005 75	0.0235	55
1000	26.7	2.3	0.75	0.007 55	0.024	52
1333.521	25	2.5	0.72	0.0094	0.024	49.5
1778.279	23.4	2.6	0.68	0.0109	0.0233	46.5
2371.373	21.8	2.75	0.63	0.0123	0.0227	43.5
3162.277	20.4	2.85	0.59	0.0134	0.0217	40.4
4216.965	18.7	2.9	0.55	0.0143	0.0207	37.6
5623.413	17.2	2.95	0.52	0.015	0.0202	34.8
7498.942	15.6	3	0.48	0.0154	0.0198	31.8
10 000	13.9	3	0.44	0.0157	0.019	28.8

[a] The numbers in parentheses are the threshold energies in the center-of-mass frame.

8.2. Transport and Reaction Coefficients for Ar^+ in Ar

Figure 8 shows calculated and measured drift velocities, energies, and excitation and ionization coefficients for Ar^+ in Ar. The procedures used for the calculation of transport coefficients for Ar^+ in Ar at high E/n are discussed in detail by Phelps and Jelenković.[2] They make the assumption that the ions are in equilibrium with the applied electric field and so have a one-dimensional Maxwellian energy distribution determined by the E/n value and the charge transfer cross section shown in Fig. 7. The spatial excitation and ionization coefficients in Fig. 8 and Table 8 are then averages over the respective cross sections from Fig. 7 and will be referred to as average cross sections $\bar{Q}$.

Direct comparisons with experiment can be made only for the drift velocity of Ar^+ in Ar. Thus the points of Fig. 8 show measured drift velocities,[14,61] while the solid line shows the values calculated using the charge transfer cross sections of Fig. 7 and the simple theory appropriate to a slowly varying charge transfer cross section.[15,48] The agreement in the overlapping range of E/n is expected since the cross sections in this energy range are those derived from drift velocity data.[61] Again, the one-dimensional ion velocity distribution means that the average Ar^+ energies are equal to one half the ion "temperature."

The dashed curve of average cross section for the production of the 811-nm lines is calculated from the dashed curve of Fig. 7. Note that this average cross section is much smaller than the average cross section for 811-nm production in Ar–Ar collisions. See Sec. 9.2.

The average cross section for electron production

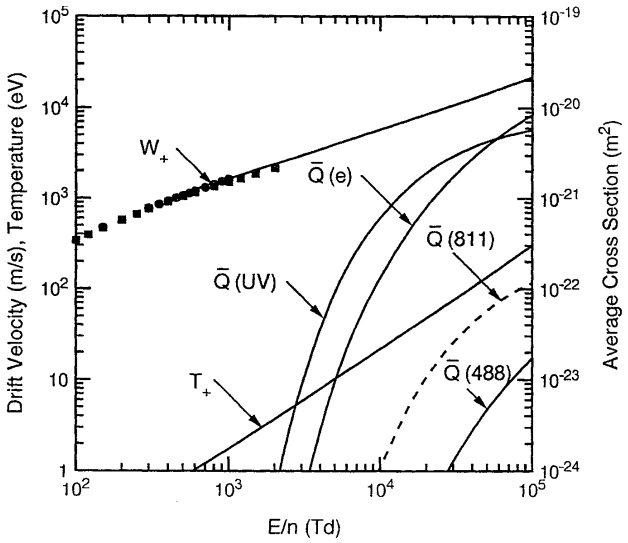

FIG. 8. Transport coefficients and average cross sections for Ar^+ in Ar as a function of E/n. The symbols and calculated quantities are: W_+, ion drift velocity; T_+, ion temperature; $\bar{Q}$(UV), Ar UV excitation; $\bar{Q}$(488), ArII excitation at 488 nm; $\bar{Q}(e)$, electron production; $\bar{Q}$(811), estimated Ar 811-nm excitation. Experimental drift velocities are indicated by ■ from Ref. 14 and ● from Ref. 62. The Ar 811-nm excitation curve is shown dashed because of the uncertainty in its estimate from the Ne 614-nm excitation cross section.

shown by the solid curve of Fig. 8 was used by Jelenković and Phelps[3] in models of measured breakdown voltages in Ar at very high E/n. However, the Ar^+ flux densities were too small compared to the fast Ar flux densities to provide a test of the Ar^+ ionization coefficients.[3]

TABLE 8. Calculated drift velocities, steady-state energies and reaction coefficients for Ar^+ in Ar.

E/n Td	Q_{CT} m²	T_+ eV	W_+ m/s	$\bar{Q}(e)$ m²	$\bar{Q}$(UV) m²	$\bar{Q}$(488) m²	$\bar{Q}$(811) m²
500	5.8E–19[a]	0.862	1150	...[b]	...	...	...
1000	5.7E–19	1.754	1641	8.22E–31	1.67E–28	...	...
2000	5.4E–19	3.70	2380	1.28E–26	5.13E–25	1.02E–35	1.13E–31
3000	5.2E–19	5.77	2980	4.40E–25	8.55E–24	1.05E–31	1.06E–28
5000	4.9E–19	10.20	3960	9.45E–24	9.10E–23	1.23E–28	2.15E–26
10 000	4.6E–19	21.7	5780	1.32E–22	6.08E–22	1.85E–26	1.08E–24
20 000	4.2E–19	47.6	8550	8.02E–22	1.91E–21	3.62E–25	1.06E–23
30 000	4.0E–19	75	10 730	1.73E–21	2.92E–21	1.27E–24	2.56E–23
50 000	3.7E–19	135.1	14 400	3.81E–21	4.26E–21	4.67E–24	8.79E–23
100 000	3.3E–19	303	21 600	8.48E–21	5.75E–21	1.74E–23	1.16E–22

[a] Too small for meaningful calculation.
[b] 5.8E–19 means 5.8×10^{-19}.

9. Ar Collisions with Ar

9.1. Ar–Ar Cross Sections

The cross section set for fast Ar collisions with Ar is shown in Fig. 9 and listed in Table 9. The momentum transfer cross sections shown for Ar–Ar collisions at $\epsilon_L > 10$ eV were calculated by Robinson[71] from differential scattering data. The cross sections for $\epsilon_L < 10$ eV are chosen to make a smooth transition from Robinson's values to cross sections calculated from experimental[57] and theoretical[72] diffusion coefficients at thermal energies.

The sum of the cross sections for excitation of the 104.8 and 106.7-nm resonance lines[73] are shown in Fig. 9. Since this sum is fortuitously equal to the ionization cross section to within the scatter only one entry is given in Table 9. A significant fraction of the resonance line production is attributed by Kempter *et al.*[74] to cascading from higher levels.

The excitation of radiative transitions from the $3p_n$ and $2p_n$ levels to the $1s_n$ levels of Ar in Ar–Ar collisions has been reported by Neuman[75] and by Kempter *et al.*[76] The only energy dependent cross section given[76] for the Ar $2p_n$ lines is that shown in Fig. 9 for the 795-nm line. The point shown for the combined 811.5 and 810.4-nm lines at 900 eV was obtained by multiplying the 795-nm cross section by the ratio of the 811 to 795-nm intensities measured by Kempter *et al.*[76] The curve designated by $Q(811)$ in Fig. 9 is that obtained by Phelps and Jelenković[2] by adjusting the lower energy portion of the 811-nm cross section to yield excitation coefficients consistent with their experiment while passing through the point[76] at 900 eV.

Estimates of cross sections for excitation of metastable Ar in Ar–Ar collisions have been obtained for $\epsilon_L < 32$ eV from beam techniques.[77] These cross sections are too small to be shown in Fig. 9. Values inferred from the growth of ionization in shock tubes are questionable.[78,79] Low angle, high energy resolution measurements[80] of the scattering of Ar by Ar demonstrate the dominance of excitation to the $1s$ and $2p$ configurations of Ar at high energies, but neither experiment nor theory[80,81] gives information as to the ratio of cross sections for metastable and resonance-line excitation. As for Ar^+, we estimate the cross sections for excitation of Ar to the metastable states by fast Ar to be less than or equal to those for resonance-line excitation in Ar–Ar collisions.

The electron production cross section for Ar–Ar collisions $Q(e)$ has been measured by several authors[70,77,82–84] and is shown in Fig. 9 and listed in Table 9.

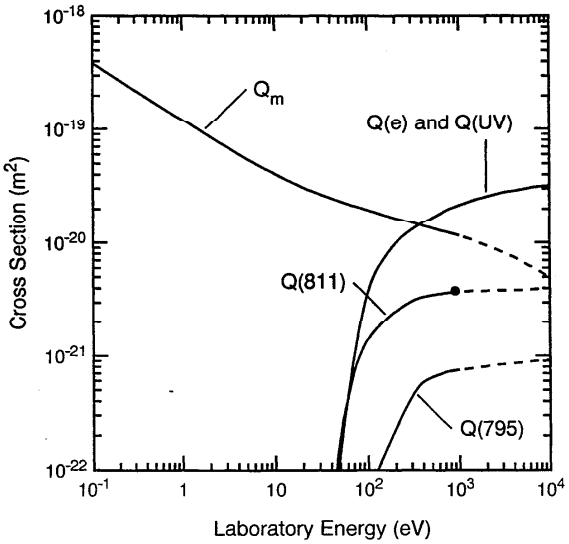

FIG. 9. Cross sections for Ar–Ar collisions versus laboratory energy. The symbols and collision process are: Q_m, momentum transfer cross section; $Q(e)$, electron production; $Q(\mathrm{UV})$, UV excitation cross section; $Q(811)$, excitation cross section for 811-nm line of Ar; and $Q(795)$, cross section for production of the 795-nm line of Ar. The point ● is from Refs. 74 and 76.

TABLE 9. Cross sections for Ar + Ar collisions tabulated by product. (Cross sections in units of 10^{-20} m^2.)

Lab. atom energy eV	Cross section $Q(\mathrm{UV})$ and $Q(e)$(11.6) and (15.8)[a]	$Q(811)$ (13.1)	$Q(795)$ (11.6)	Q_m
0.1				38.5
0.1334				33.2
0.1778				28.8
0.237				24.9
0.316				21.7
0.422				18.7
0.562				16.1
0.750				14.1
1				12.2
1.334				10.6
1.778				9.1
2.37				7.9
3.16				6.85
4.22				5.9
5.62				5.2
7.50				4.63
10				4.07
13.34				3.65
17.78				3.27
23.7				2.94
31.6				2.67
42.2	0.003	0.006		2.42
56.2	0.03	0.033		2.26
75.0	0.13	0.085	0.0025	2.09
100	0.37	0.14	0.0063	1.95
133.4	0.63	0.185	0.0111	1.81
177.8	0.88	0.235	0.0189	1.7
237	1.12	0.285	0.0305	1.59
316	1.33	0.315	0.0467	1.49
422	1.54	0.34	0.0605	1.4
562	1.74	0.355	0.0673	1.32
750	1.96	0.365	0.0725	1.23
1000	2.14	0.37	0.075	1.15
1334	2.33	0.38	0.0775	1.07
1778	2.5	0.38	0.08	0.98
2370	2.64	0.385	0.0825	0.895
3160	2.8	0.385	0.0845	0.807
4220	2.9	0.387	0.0865	0.735
5620	3.03	0.39	0.0887	0.645
7500	3.13	0.395	0.0905	0.57
10 000	3.2	0.4	0.092	0.49

[a] The numbers in parentheses are the threshold energies in the center-of-mass frame.

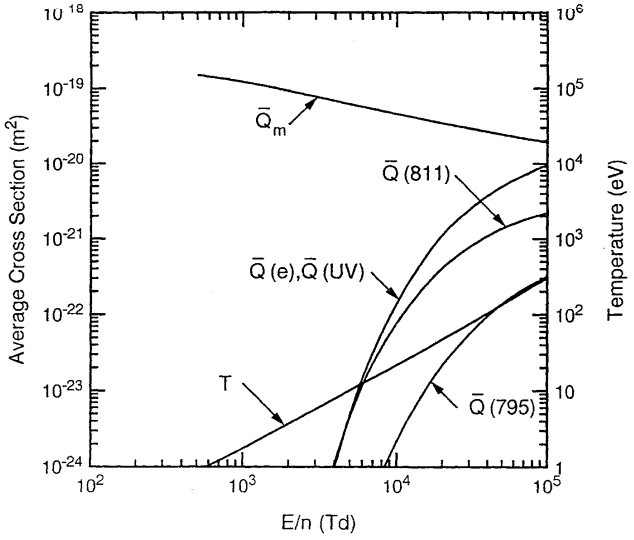

FIG. 10. Average cross sections and fast atom "temperature" as a function of E/n for fast Ar formed by charge transfer collisions from Ar^+ drifting through Ar. The symbols and calculated quantities are T, ion and initial fast atom temperature; $\bar{Q}$(UV), Ar UV excitation; $\bar{Q}$(811), Ar I excitation at 811 nm; $\bar{Q}(e)$, electron production; $\bar{Q}$(795), Ar 795-nm excitation.

9.2. Reaction Coefficients for Ar in Ar

The spatial reaction coefficients or average cross sections for ionization, excitation, and destruction in Ar–Ar collisions in Fig. 10 and listed in Table 10 were calculated using the energy distributions versus E/n calculated for Ar^+ in Ar.[2] As discussed by Phelps and Jelenković[2] this approximation is appropriate for experiments where the fast Ar are produced in charge transfer collisions of Ar^+ with Ar. The destruction coefficient curve shown is calculated assuming that any collision of fast Ar with Ar results in sufficient energy loss to remove the fast Ar from the group of atoms in the beam that are able to cause excitation or ionization. More accurate models would take into account details of the elastic, excitation, and ionization collisions which occur as the fast Ar lose energy.

The average cross section $\bar{Q}(811)$ shown for excitation of the 811-nm lines of Ar is calculated from the cross section shown by the dashed curve of Fig. 9, which is chosen to fit the drift tube experiments of Phelps and Jelenković.[2]

TABLE 10. Reaction coefficients for Ar + Ar tabulated by product.

E/n Td	T eV	$\bar{Q}(e),\bar{Q}$(UV) m²	$\bar{Q}$(811) m²	Q(795) m²	Q_m m²
500	0.862	...[a]	...	...	1.51E-19[b]
1000	1.754	...	...	...	1.22E-19
2000	3.70	1.46E-27	2.61E-27	2.47E-31	9.29E-20
3000	5.77	1.03E-25	1.46E-25	2.23E-28	7.81E-20
5000	10.20	4.90E-24	4.65E-24	4.49E-26	6.21E-20
10 000	21.7	1.41E-22	7.76E-23	2.20E-24	4.61E-20
20 000	47.6	1.13E-21	4.13E-22	2.17E-23	3.44E-20
30 000	75	2.44E-21	7.72E-22	5.53E-23	2.94E-20
50 000	135.1	4.96E-21	1.37E-21	1.39E-22	2.44E-20
100 000	303	9.56E-21	2.22E-21	3.16E-22	1.93E-20

[a] Too small for meaningful calculation.
[b] 1.51E-19 means 1.51×10^{-19}.

10. Ar_2^+ Collisions with Ar

The only data we have found on collisions of Ar_2^+ with Ar are from measurements of drift velocity[54] for $50 < E/n < 100$ Td, corresponding to ion energies up to 0.04 eV. The momentum transfer cross section required to fit this drift velocity data is about 15% larger than the "Langevin" cross section calculated from the polarizability of Ar. At $\epsilon_L > 500$ eV the scaling factor given by Eq. (1) results in a predicted cross section for Ar_2^+ with Ar which is ≈ 16 times that for N^+ with N_2 shown in Fig. 1. In view of the uncertainties, we have not shown or tabulated these estimates of Q_m. Measurements of the dissociation of Ar_2^+ in collisions with Ar at 3 keV have been reported by Stephan, Stamotović, and Märk.[85] Discussion of the data regarding the formation of Ar_2^+ in three-body collisions of Ar^+ with Ar[86] and of the Ar^+–Ar bond energy[87] is outside the scope of this paper.

11. Discussion

The cross sections compiled in this paper demonstrate the wide range of processes and of experimental and theoretical techniques that need to be considered in order to begin to assemble the "complete" sets needed for modeling. At energies below 10 eV transport and reaction measurements utilizing swarm, ion cyclotron resonance, and flow tube techniques provide much of the available experimental data. At energies above 500 eV beam scattering techniques yield detailed data such as differential scattering cross sections. The intermediate energy range is only beginning to be studied. Very few theoretical calculations of cross sections are available for the energy range of interest here. It is to be hoped that more investigations will be made of the intermediate energy range, including tests of the usefulness of relatively simple theories such as the Born approximation and simple molecular models.

The cross sections presented in this review provide the basis of modeling of electrical discharge in weakly ionized N_2 and Ar. To serve that purpose the cross sections must be "complete." It is hoped that the occasional somewhat arbitrary choices and the necessity for estimates of many of the cross sections in critical ranges will encourage experimentalists and theoreticians to carry out further work in this area.

In most cases we have cited only the publications containing data actually used. A "floppy disk" containing the tabulated data is available from the author. Please inform the author of errors, omissions, or new data.

12. Acknowledgments

The author wishes to acknowledge helpful discussions of theory and experiment with A. Gallagher and B. M. Jelenković and an unknown referee for critical comments and correcting errors in the manuscript. He wishes to thank R. C. Isler and E. G. Jones for supplying unpublished data and

the JILA Information Center for assistance with the cataloging of references. The support of the National Institute of Standards and Technology throughout this project is gratefully appreciated. The initial phase of this work were also supported by the Lawrence Livermore Laboratories.

13. References

[1]A. V. Phelps, J. Phys. Chem. Ref. Data **19**, 653 (1990).
[2]A. V. Phelps and B. M. Jelenković, Phys. Rev. A **38**, 2975 (1988).
[3]B. M. Jelenković and A. V. Phelps, Phys. Rev. A **36**, 5310 (1987).
[4]V. T.Gylys, B. M. Jelenković, and A. V. Phelps, J. Appl. Phys. **65**, 3369 (1989).
[5]M. J. Druyvesteyn and F. M. Penning, Rev. Mod. Phys. **12**, 87 (1940).
[6]G. Francis, in *Handbuch der Physik*, edited by S. Flugge (Springer, Berlin, 1956), Vol. 22, pp. 53–208.
[7]A. V. Bondarenko, Zh. Tekh. Fiz. **45**, 308 (1975) [Sov. Phys. Tech. Phys. **20**, 195 (1975)].
[8]A. V. Phelps (unpublished).
[9]D. Bloess, I. Kamber, H. Riege, G. Bittner, V. Brückner, J. Christiansen, K. Frank, W. Hartmann, N. Lieser, Ch. Schultheiss, R. Seeböck, and W. Steudtner, Nucl. Instrum. Methods **205**, 173 (1983).
[10]K. N. Ul'yanov and A. B. Tskhai, Teplofiz. Vys. Temp. **19**, 41 (1981) [High Temperature **19**, 32 (1981)].
[11]J. R. Hiskes, Comments At. Mol. Phys. **19**, 59 (1987); O. Fukumasa, R. Itatani, and S. Saeki, J. Phys. D **18**, 2433 (1985).
[12]H. Pak and M. Kushner, Bull. Am. Phys. Soc. **35**, 1824 (1990).
[13]A. V. Phelps, in *Abstracts of Contributed Papers for International Conference on the Physics of Electronic and Atomic collisions*, edited by J.Geddes, H. B. Gilbody, A. E. Kingston, C. J. Latimer, and H. R. J. Walters (North-Holland, Amsterdam, 1987), p. 690.
[14]H. W. Ellis, R. Y. Pai, E. W. McDaniel, E. A. Mason, and L. A. Viehland, At. Data Nucl. Data Tables **17**, 177 (1976).
[15]E. W. McDaniel, *Collision Phenomena in Ionized Gases* (Wiley, New York, 1964), pp. 19, 71–75.
[16]E. W. McDaniel and E. A. Mason, *The Mobility and Diffusion of Ions in Gases* (Wiley, New York, 1973), p. 344.
[17]J. H. Newman, Y. S. Chen, K. A. Smith, and R. F. Stebbings, J. Geophys. Res. **91**, 8947 (1986); J. H. Newman, Y. S. Chen, K. A. Smith, and R. F. Stebbings, J. Geophys. Res. **94**, 7019 (1989).
[18]D. A. Schafer, J. H. Newman, K. A. Smith, and R. F. Stebbings, J. Geophys. Res. **92**, 6107 (1987).
[19]E. W. McDaniel, *Atomic Collisions: Electron and Photon Projectiles* (Wiley, New York, 1989), p. 94.
[20]E. Gustafsson and E. Lindholm, Ark. Fys. **18**, 219 (1960).
[21]R. F. Potter, J. Chem. Phys. **22**, 974 (1954).
[22]W. B. Maier II and E. Murad, J. Chem. Phys. **55**, 2307 (1971).
[23]R. F. Stebbings, B. R. Turner, and A. C. H. Smith, J. Chem. Phys. **38**, 2277 (1963).
[24]G. J. Lockwood, G. H. Miller, and J. M. Hoffman, Phys. Rev. A **18**, 935 (1978); J. M. Hoffman, G. H. Miller, and G. J. Lockwood, Phys. Rev. A **25**, 1930 (1982).
[25]T. F. Moran and J. B. Wilcox, J. Chem. Phys. **70**, 1467 (1979); T. F. Moran and B. P. Mathur, Phys. Rev. A **21**, 1051 (1980).
[26]C. Ottinger and J. Simonis, Chem. Phys. **28**, 97 (1978).
[27]J. R. Sheridan and K. C. Clark, Phys. Rev. **140**, A1033 (1965).
[28]J. H. Moore, Jr., and J. P. Doering, Phys. Rev. **177**, 218 (1969).
[29]V. M. Lavrov, M. R. Gochitashvili, V. A. Ankudinov, and B. I. Kikiani, Zh. Tekh. Fiz. **50**, 660 (1980) [Sov. Phys. Tech. Phys. **25**, 400 (1980)].
[30]J. H. Moore, Jr., Phys. Rev. **8**, 2359 (1973).
[31]N. Kobayashi, J. Phys. Soc. Jpn. **38**, 519 (1975).
[32]T. Holstein, J. Phys. Chem. **56**, 832 (1952).
[33]B. Friedrich, S. L. Howard, A. L. Rockwood, W. E. Trafton, Jr., D. Wen-Hu, and J. H. Futrell, Int. J. Mass Spectrom. Ion Proc. **59**, 203 (1984).
[34]A. Ding and K. Richter, Z. Phys. A **307**, 31 (1982).
[35]T. F. Moran, K. J. McCann and M. R. Flannery, J. Chem. Phys. **63**, 3857 (1975).
[36]K. B. McAfee, Jr., C. R. Szmanda, R. S. Hozack, and R. E. Johnson, J. Chem. Phys. **77**, 2399 (1982).
[37]W. Lindinger, F. Howorka, P. Lukac, S. Kuhn, H. Villinger, E. Alge, and H. Ramler, Phys. Rev. A **23**, 2319 (1981); D. Smith and N. G. Adams, Phys. Rev. A **23**, 2327 (1981); E. E. Ferguson, J. Phys. Chem. **90**, 731 (1986).
[38]A. C. G. Mitchell and M. W. Zemansky, *Resonance Radiation and Excited Atoms* (Cambridge U.P., Cambridge, 1934), pp. 57–59.
[39]W. B. Maier II, J. Chem Phys. **55**, 2699 (1971); **61**, 3459 (1974).
[40]T. F. Moran, J. B. Wilcox, and L. E. Abbey, J. Chem. Phys. **65**, 4540 (1976).
[41]J. J. Leventhal and L. Friedman, J. Chem. Phys. **46**, 997 (1967).
[42]V. Čermák and Z. Herman, Collect. Czech. Chem. Commun. **27**, 1493 (1962).
[43]M. C. Cress, P. M. Becker, and F. W. Lampe, J. Chem Phys. **44**, 2212 (1966); R. K. Asundi, G. J. Schulz, and P. J. Chantry, J. Chem. Phys. **47**, 1584 (1967).
[44]S. H. Neff, Astrophys. J. **140**, 348 (1964).
[45]J. P. Doering, Phys. Rev. **133**, A1537 (1964).
[46]C. Liu and H. P. Broida, Phys. Rev. A **2**, 1824 (1970).
[47]N. G. Utterback and B. Van Zyl, J. Chem. Phys. **68**, 2742 (1978). See also N. G. Utterbach and G. H. Miller, Phys. Rev. **124**, 1477 (1961); H. H. Fleischmann and R. A. Young, Phys. Rev. **178**, 254 (1969).
[48]J. E. Lawler, Phys. Rev. A **32**, 2977 (1985).
[49]J. Borysow and A. V. Phelps, Bull Am. Phys. Soc. **35**, 1837 (1990).
[50]J. Fletcher and H. A. Blevin, J. Phys. D **14**, 27 (1981).
[51]J. T. Moseley, R. M. Snuggs, D. W. Martin, and E. W. McDaniel, Phys. Rev. **178**, 240 (1969).
[52]L. G. McKnight, K. B. McAfee, and D. P. Sipler, Phys. Rev. **164**, 62 (1967).
[53]M. Saporoschenko, Phys. Rev. **111**, 1550 (1958).
[54]H. W. Ellis, M. G. Thackston, E. W. McDaniel, and E. A. Mason, At. Data Nucl. Data Tables **31**, 113 (1984).
[55]R. N. Varney, Phys. Rev. **174**, 165 (1968); D. Smith, N. G. Adams, and E. Alge, Chem. Phys. Lett. **105**, 317 (1984); B. R. Rowe, G. Dupeyrat, J. B. Marquette, and P. Gaucherel, J. Chem. Phys. **80**, 4915 (1984).
[56]A. Laganà, E. Garcia, and L. Ciccarelli, J. Phys. Chem. **91**, 312 (1987).
[57]S. Chapman and T. G. Cowling, *The Mathematical Theory of Non-Uniform Gases* (Cambridge U.P., Cambridge, 1970), p. 267.
[58]R. L. Taylor and S. Bitterman, Rev. Mod. Phys. **41**, 26 (1969).
[59]D. Rapp and T. Kassal, Chem. Rev. **69**, 61 (1969).
[60]J. R. Sheridan and J. R. Peterson, J. Chem Phys. **51**, 3574 (1969).
[61]R. Hegerberg, M. T. Elford, and H. R. Skullerud, J. Phys. B **15**, 797 (1982).
[62]E. Salzborn, IEEE Trans. Nucl. Sci. **NS-23**, 947 (1976).
[63]R. C. Isler and L. E. Murray, in *Electronic and Atomic Collisions*, edited by J. S. Risley and R. Geballe (Univ. of Washington, Seattle, 1975), Vol. 2, p. 609; R. C. Isler (private communication, 1986).
[64]P. O. Haugsjaa, R. C. Amme, and N. G. Utterback, Phys. Rev. Lett. **22**, 322 (1969).
[65]V. Sidis, M. Barat, and D. Dhuicq, J. Phys. B **8**, 474 (1975).
[66]C. E. Moore, *Atomic Energy Levels* (U. S. Department of Commerce, Washington, 1949), Vol. 1, Cir. 467.
[67]Th. J. M. Sluyters and J. Kistermacher, Physica (Utrecht) **25**, 1389 (1959).
[68]S. N. Neff, Astrophys. J. **140**, 348 (1964).
[69]E. G. Jones, Phys. Rev. A **21**, 1902 (1980); E. G. Jones, Air Force Aeropropulsion Laboratory Report, No. AFAPL-TR-78-99, 1978 (unpublished)
[70]Th. J. M. Sluyters, E. De Hass, and J. Kistermacher, Physica (Utrecht) **25**, 1376 (1959).
[71]R. S. Robinson, J. Vacuum Sci. Technol. **16**, 185 (1979).
[72]J. H. Dymond, J. Phys. B **4**, 621 (1971).
[73]H. L. Rothwell, Jr., R. C. Amme, and B. Van Zyl, Phys. Rev. A **19**, 970 (1979).
[74]V. Kempter, G. Riecke, F. Vieth, and L. Zehnle, J. Phys. B **9**, 3081 (1975).
[75]V. Neuman, Ann. Phys. (Leipzig) **34**, 603 (1939).
[76]V. Kempter, F. Vieth, and L. Zehnle, J. Phys. B **8**, 2835 (1975).
[77]P. O. Haugsjaa and R. C. Amme, J. Chem. Phys. **52**, 4874 (1970).
[78]T. I. McLaren and R. M. Hobson, Phys. Fluids **11**, 2162 (1968). Using detailed balancing arguments and measured Ar metastable two-body destruction rate coefficients, we conclude that these excitation cross sections are much too large. The same conclusion has been reached by Botticher, who presents evidence that the effect is caused by impurities (see Ref. 79).
[79]W. Botticher, in *Invited Papers from the International Conference on Ionization Phenomena in Gases*, edited by W. T. Williams (Hilger, Bristol, 1987), p. 10.
[80]J. C. Brenot, D. Dhuicq, J. P. Gauyacq, J. Pommier, V. Sidis, M. Barat, and E. Pollack, Phys. Rev. A **11**, 1245 (1975).
[81]J. P. Gauyacq, J. Phys. B **11**, 85 (1978).

[82]H. C. Hayden and R. C. Amme, Phys. Rev. **141**, 30 (1966).
[83]R. H. Hammond, J. M. S. Henis, E. F. Greene, and J. Ross, J. Chem. Phys. **55**, 3506 (1971).
[84]P. O. Haugsjaa and R. C. Amme, Phys. Rev. Lett. **23**, 633 (1969).
[85]K. Stephan, A. Stamatović, and T. D. Märk, Phys. Rev. A **28**, 3105 (1983).
[86]R. Johnsen, A. Chen, and M. A. Biondi, J. Chem. Phys. **73**, 1717 (1980); M. Grössi, M. Langenwalter, H. Helm, and T. D. Märk, J. Chem. Phys. **74**, 1728 (1981).
[87]R. G. Keesee and A. W. Castelman, Jr., J. Phys. Chem. Ref. Data **15**, 1011 (1986).